Supplementary: Heat transport and flow morphology of geostrophic rotating Rayleigh-Bénard convection in the presence of boundary flow

Guang-Yu Ding[1,2] and Ke-Qing Xia[1]
[1] *Center for Complex Flows and Soft Matter Research and Department of Mechanics and Aerospace Engineering, Southern University of Science and Technology, Shenzhen,518055, China and*
[2] *Department of Physics, The Chinese University of Hong Kong, Hong Kong, China*

In tables S1-S4, we list the parameters and the numerical setups in this study. In these tables, N_z, N_ϕ and N_r respectively refer to the number of grids for the vertical (z), azimuthal (ϕ) and radial (r) direction for the momentum solver. The superscript s denotes the number of grids for the temperature solver. To validate the meshes used in the study, we compare the vertical grid spacing with the Kolmogorov and Batchelor length scales. In the current study, the dimensionless Kolmogorov length scale η_k is evaluated using

$$\eta_k = \left[\frac{Ra}{Pr}\left(\frac{\partial u_i}{\partial x_j}\right)^2\right]^{-1/4}. \tag{1}$$

and the dimensionless Batchelor length scale is evaluated using $\eta_b = \eta_k/\sqrt{Pr}$. Here we respectively define R_k and R_b as the grid spacing ratio for the velocity and temperature field.

$$R_k \equiv \max(dZ/\langle R_k\rangle_{r,\phi}), \qquad R_b \equiv \max(dZs/\langle R_b\rangle_{r,\phi}), \tag{2}$$

where dZ and dZs are the vertical grid spacing for the coarse (velocity) meshes and dense (temperature) meshes, respectively. The ratios R_k and R_b are listed in the following tables. In most cases, these ratios are less than 1, indicating that our resolution is adequate for capturing the small-scale structures in this system. Even for cases where the ratios are greater than 1, their values remain reasonably close to unity, suggesting that the resolution is still sufficient.

For high rotation rate, the viscous dissipation decreases drastically as the Taylor-Proudman effect suppress the flow strength, leading to the increase of Kolmogorov and Batchelor length scales. On the other hand, the Ekman boundary layer decreases as Ek decreases, following the scaling law $\delta_{Ek} \sim Ek^{1/2}$. Thus, comparing the grid spacing with the Kolmogorov and Batchelor length scales may not be able to validate the grids in high rotation rate. To examine the grid spacing for high rotation rate, we focus on the case with the minimum Ek (or minimum Ra/Ra_c for Set I) in this study, which exhibits the thinnest Ekman layer $\delta_{Ek} \sim Ek^{1/2}$ and has the highest likelihood of encountering resolution issues in the boundary layer, if any exist. We select two cases to check the grid spacing in the boundary

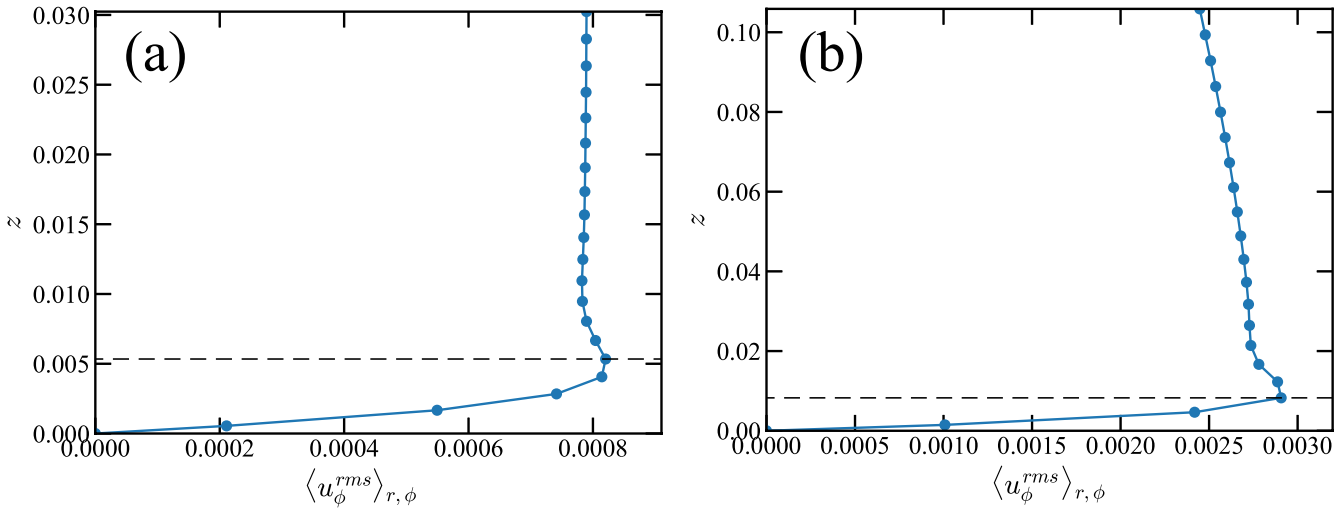

FIG. S1: The root mean square u_ϕ^{rms} of the azimuthal velocity averaged over the azimuthal and radial directions for (a) $Ra = 2\times10^7$, $Ek = 1.85\times10^{-6}$, and $Fr = 0$ in Set I, and (b) $Ra = 2\times10^7$ and $Ek = 9.20\times10^{-6}$ in Set III. The dashed line indicates the maximum of u_ϕ^{rms}, which corresponds to the location of the Ekman boundary layer.

Γ	Ra	Ek	Ra/Ra_c	Ra/Ra_w	Fr	N_z	N_ϕ	N_r	N_z^s	N_ϕ^s	N_r^s	R_k	R_b
0.5	2.00×10^7	1.85×10^{-6}	0.06	1.14	0	384	144	36	384	288	74	0.07	0.14
0.5	2.30×10^7	1.85×10^{-6}	0.07	1.31	0	384	144	36	384	288	74	0.08	0.17
0.5	2.80×10^7	1.85×10^{-6}	0.08	1.60	0	384	144	36	384	288	74	0.10	0.20
0.5	4.00×10^7	1.85×10^{-6}	0.12	2.29	0	384	144	36	384	288	74	0.12	0.25
0.5	5.50×10^7	1.85×10^{-6}	0.16	3.14	0	384	144	36	384	288	74	0.14	0.30
0.5	8.00×10^7	1.85×10^{-6}	0.24	4.57	0	384	144	36	384	288	74	0.17	0.35
0.5	1.27×10^8	1.85×10^{-6}	0.38	7.26	0	512	192	48	512	384	96	0.15	0.32
0.5	2.15×10^8	1.85×10^{-6}	0.64	12.29	0	512	192	48	512	384	96	0.18	0.38
0.5	3.40×10^8	1.85×10^{-6}	1.01	19.43	0	512	192	48	512	384	96	0.21	0.45
0.5	5.12×10^8	1.85×10^{-6}	1.52	29.26	0	512	192	48	512	384	96	0.26	0.54
0.5	6.97×10^8	1.85×10^{-6}	2.07	39.83	0	576	192	48	576	384	96	0.28	0.59
0.5	8.71×10^8	1.85×10^{-6}	2.59	49.78	0	576	192	48	576	384	96	0.35	0.74
0.5	1.02×10^9	1.85×10^{-6}	3.03	58.29	0	576	192	48	576	384	96	0.42	0.88
0.5	1.30×10^9	1.85×10^{-6}	3.87	74.29	0	576	256	64	576	512	128	0.50	1.04
0.5	1.54×10^9	1.85×10^{-6}	4.58	88.01	0	640	256	64	640	512	128	0.50	1.05
0.5	3.07×10^9	1.85×10^{-6}	9.13	175.44	0	704	256	64	704	512	128	0.62	1.29
1	2.00×10^7	1.85×10^{-6}	0.06	1.14	0	384	288	64	384	576	128	0.05	0.11
1	2.80×10^7	1.85×10^{-6}	0.08	1.60	0	384	288	64	384	576	128	0.08	0.17
1	4.00×10^7	1.85×10^{-6}	0.12	2.29	0	384	288	64	384	576	128	0.11	0.22
1	8.00×10^7	1.85×10^{-6}	0.24	4.57	0	384	288	64	384	576	128	0.39	0.81
1	1.27×10^8	1.85×10^{-6}	0.38	7.26	0	384	288	64	384	576	128	0.40	0.84
1	2.15×10^8	1.85×10^{-6}	0.64	12.29	0	384	288	64	384	576	128	0.46	0.96
1	2.84×10^8	1.85×10^{-6}	0.84	16.23	0	384	288	64	384	576	128	0.48	1.01
1	3.40×10^8	1.85×10^{-6}	1.01	19.43	0	384	288	64	384	576	128	0.48	1.00
1	4.00×10^8	1.85×10^{-6}	1.19	22.86	0	512	384	86	512	768	172	0.39	0.81
1	5.12×10^8	1.85×10^{-6}	1.52	29.26	0	512	384	86	512	768	172	0.33	0.69
1	6.97×10^8	1.85×10^{-6}	2.07	39.83	0	512	384	86	512	768	172	0.31	0.65
1	8.71×10^8	1.85×10^{-6}	2.59	49.78	0	576	384	96	576	768	192	0.35	0.72
1	1.02×10^9	1.85×10^{-6}	3.03	58.29	0	576	384	96	576	768	192	0.42	0.88
1	1.30×10^9	1.85×10^{-6}	3.87	74.29	0	576	512	128	576	1024	256	0.50	1.04
1	1.54×10^9	1.85×10^{-6}	4.58	88.01	0	640	512	128	640	1024	256	0.51	1.06
1	3.07×10^9	1.85×10^{-6}	9.13	175.44	0	704	512	128	704	1024	256	0.57	1.20
2	4.00×10^7	1.85×10^{-6}	0.12	2.29	0	512	384	96	512	768	192	0.07	0.14
2	8.00×10^7	1.85×10^{-6}	0.24	4.57	0	512	768	192	512	1536	384	0.10	0.21
2	1.27×10^8	1.85×10^{-6}	0.38	7.26	0	512	768	192	512	1536	384	0.12	0.25
2	2.15×10^8	1.85×10^{-6}	0.64	12.29	0	512	768	192	512	1536	384	0.15	0.32
2	3.40×10^8	1.85×10^{-6}	1.01	19.43	0	512	768	192	512	1536	384	0.19	0.39
2	5.12×10^8	1.85×10^{-6}	1.52	29.26	0	512	768	192	512	1536	384	0.24	0.50
2	6.97×10^8	1.85×10^{-6}	2.07	39.83	0	576	768	192	576	1536	384	0.28	0.58
2	8.71×10^8	1.85×10^{-6}	2.59	49.78	0	576	768	192	576	1536	384	0.35	0.74
2	1.02×10^9	1.85×10^{-6}	3.03	58.29	0	576	1024	256	576	2048	512	0.44	0.92
2	1.30×10^9	1.85×10^{-6}	3.87	74.29	0	576	1024	256	576	2048	512	0.50	1.05
2	3.07×10^9	1.85×10^{-6}	9.13	175.44	0	704	1024	256	704	2048	512	0.58	1.21

TABLE S1: Numerical setup for the cases in Set I.

layer: $Ra = 2\times10^7$, $Ek = 1.85\times10^{-6}$, and $Fr = 0$ in Set I, and $Ra = 2\times10^7$ and $Ek = 9.20\times10^{-6}$ in Set III. For the former case, there are 6 grid points within the Ekman boundary layer (see Fig. S1a). As for the latter, there are 4 grid points within the boundary layer (see Fig. S1b). These results reasonably demonstrate that the grid resolution we employed in this study is sufficient to revolve the fine structures either in high or low rotation rates.

Γ	Ra	Ek	Ra/Ra_c	Ra/Ra_w	Fr	N_z	N_ϕ	N_r	N_z^s	N_ϕ^s	N_r^s	R_k	R_b
0.5	3.40×10^8	1.85×10^{-6}	1.01	19.43	0.06	512	192	48	512	384	96	0.21	0.44
0.5	4.00×10^8	1.85×10^{-6}	1.19	22.86	0.06	512	192	48	512	384	96	0.23	0.48
0.5	5.12×10^8	1.85×10^{-6}	1.52	29.26	0.06	512	192	48	512	384	96	0.45	0.95
0.5	6.97×10^8	1.85×10^{-6}	2.07	39.83	0.06	512	192	48	512	384	96	0.53	1.10
0.5	8.71×10^8	1.85×10^{-6}	2.59	49.78	0.06	576	192	48	576	384	96	0.48	0.99
0.5	1.02×10^9	1.85×10^{-6}	3.03	58.29	0.06	576	192	48	576	384	96	0.50	1.04
0.5	1.30×10^9	1.85×10^{-6}	3.87	74.29	0.06	576	256	64	576	512	128	0.53	1.12
0.5	1.54×10^9	1.85×10^{-6}	4.58	88.01	0.06	640	256	64	640	512	128	0.53	1.10
0.5	2.05×10^9	1.85×10^{-6}	6.10	117.15	0.06	640	256	64	640	512	128	0.59	1.24
0.5	3.07×10^9	1.85×10^{-6}	9.13	175.44	0.06	704	256	64	704	512	128	0.63	1.31
0.5	5.14×10^9	1.85×10^{-6}	15.3	293.74	0.06	768	288	72	768	576	144	0.63	1.32
0.5	9.02×10^9	1.85×10^{-6}	26.8	515.48	0.06	1024	384	96	1024	768	192	0.55	1.16
1	3.40×10^8	1.85×10^{-6}	1.01	19.43	0.12	512	384	86	512	768	172	0.40	0.84
1	4.00×10^8	1.85×10^{-6}	1.19	22.86	0.12	512	384	86	512	768	172	0.22	0.45
1	5.12×10^8	1.85×10^{-6}	1.52	29.26	0.12	512	384	86	512	768	172	0.25	0.52
1	6.97×10^8	1.85×10^{-6}	2.07	39.83	0.12	512	384	86	512	768	172	0.32	0.67
1	8.71×10^8	1.85×10^{-6}	2.59	49.78	0.12	576	384	96	576	768	192	0.36	0.76
1	1.02×10^9	1.85×10^{-6}	3.03	58.29	0.12	576	384	96	576	768	192	0.42	0.87
1	1.30×10^9	1.85×10^{-6}	3.87	74.29	0.12	576	512	128	576	1024	256	0.49	1.02
1	1.54×10^9	1.85×10^{-6}	4.58	88.01	0.12	640	512	128	640	1024	256	0.50	1.04
1	3.07×10^9	1.85×10^{-6}	9.13	175.44	0.12	704	512	128	704	1024	256	0.58	1.21
1	5.14×10^9	1.85×10^{-6}	15.3	293.74	0.12	768	576	144	768	1152	288	0.63	1.31
2	3.40×10^8	1.85×10^{-6}	1.01	19.43	0.24	512	768	192	512	1536	384	0.19	0.40
2	5.12×10^8	1.85×10^{-6}	1.52	29.26	0.24	512	768	192	512	1536	384	0.23	0.48
2	6.97×10^8	1.85×10^{-6}	2.07	39.83	0.24	512	768	192	512	1536	384	0.29	0.61
2	8.71×10^8	1.85×10^{-6}	2.59	49.78	0.24	576	768	192	576	1536	384	0.38	0.79
2	1.02×10^9	1.85×10^{-6}	3.03	58.29	0.24	576	1024	256	576	2048	512	0.41	0.85
2	1.30×10^9	1.85×10^{-6}	3.87	74.29	0.24	576	1024	256	576	2048	512	0.45	0.94
2	1.54×10^9	1.85×10^{-6}	4.58	88.01	0.24	640	1024	256	640	2048	512	0.46	0.96
2	3.07×10^9	1.85×10^{-6}	9.13	175.44	0.24	704	1024	256	704	2048	512	0.57	1.20

TABLE S2: Numerical setup for the cases in Set II.

Γ	Ra	Ek	Ra/Ra_c	N_z	N_ϕ	N_r	N_z^s	N_ϕ^s	N_r^s	R_k	R_b
1.0	4.00×10^8	1.85×10^{-6}	1.19	256	192	192	512	384	384	0.02	0.02
1.0	4.57×10^8	1.85×10^{-6}	1.36	256	192	192	512	384	384	0.39	0.41
1.0	5.12×10^8	1.85×10^{-6}	1.52	256	192	192	512	384	384	0.50	0.52
1.0	6.00×10^8	1.85×10^{-6}	1.79	256	192	192	512	384	384	0.63	0.66
1.0	6.97×10^8	1.85×10^{-6}	2.07	256	192	192	512	384	384	0.73	0.76
1.0	8.71×10^8	1.85×10^{-6}	2.59	256	192	192	512	384	384	0.88	0.92
1.0	1.02×10^8	1.85×10^{-6}	3.03	256	192	192	512	384	384	1.00	1.05
1.0	1.30×10^8	1.85×10^{-6}	3.87	256	192	192	512	384	384	1.16	1.22
1.0	1.54×10^8	1.85×10^{-6}	4.58	256	192	192	512	384	384	1.27	1.33

TABLE S3: Numerical setup for the cases using lateral periodic boundary conditions.

Ra	Ek	Ra/Ra_c	Ra/Ra_w	Fr	N_z	N_ϕ	N_r	N_z^s	N_ϕ^s	N_r^s	R_k	R_b
2.00×10^7	9.20×10^{-6}	0.53	5.61	0.0	160	384	140	160	768	280	0.19	0.39
2.00×10^7	1.15×10^{-5}	0.72	7.00	0.0	160	384	140	160	768	280	0.20	0.42
2.00×10^7	1.43×10^{-5}	0.96	8.68	0.0	160	384	140	160	768	280	0.21	0.44
2.00×10^7	1.78×10^{-5}	1.30	10.78	0.0	160	384	140	160	768	280	0.24	0.51
2.00×10^7	1.90×10^{-5}	1.42	11.50	0.0	160	384	140	160	768	280	0.26	0.55
2.00×10^7	2.22×10^{-5}	1.76	13.41	0.0	160	384	140	160	768	280	0.32	0.67
2.00×10^7	2.66×10^{-5}	2.26	16.03	0.0	160	384	140	160	768	280	0.37	0.78
2.00×10^7	3.33×10^{-5}	3.07	20.00	0.0	160	384	140	160	768	280	0.44	0.91
2.00×10^7	3.67×10^{-5}	3.51	22.01	0.0	160	384	140	160	768	280	0.45	0.94
2.00×10^7	4.44×10^{-5}	4.57	26.55	0.0	160	384	140	160	768	280	0.46	0.97
2.00×10^7	5.41×10^{-5}	5.99	32.24	0.0	160	384	140	160	768	280	0.47	0.98
2.00×10^7	9.18×10^{-5}	12.45	54.16	0.0	160	384	140	160	768	280	0.46	0.95

TABLE S4: Numerical setup for the cases of Set III.